Inorg. Chem. **2003**, *42*, 2950–2959

Self-Assembled Dinuclear, Trinuclear, Tetranuclear, Pentanuclear, and Octanuclear Ni(II) Complexes of a Series of Polytopic Diazine Based Ligands: Structural and Magnetic Properties

Zhiqiang Xu, Laurence K. Thompson,* Victoria A. Milway, Liang Zhao, Timothy Kelly, and David O. Miller

Department of Chemistry, Memorial University of Newfoundland, St. John's, Newfoundland, Canada A1B 3X7

Received December 2, 2002

The nickel coordination chemistry of a series of polytopic diazine (N–N) based ligands has been examined. Self-assembly reactions lead to examples of dinuclear, trinuclear, tetranuclear, pentanuclear, and octanuclear complexes, all of which exhibit magnetic exchange coupling, with antiferromagnetic and ferromagnetic examples. Structural details are presented for $[(L1)_2Ni_2(H_2O)_2](NO_3)_4 \cdot 3H_2O$ (**1**), $[(L2)_2Ni_3(H_2O)_2](NO_3)_6 \cdot 8H_2O$ (**2**), $[(L3)_4Ni_4(H_2O)_8](NO_3)_4 \cdot 8H_2O$ (**3**), $[(L4)_2Ni_5(H_2O)_{10}(NO_3)](NO_3)_7 \cdot 8H_2O$ (**4**), and $[(L5)_4Ni_8(H_2O)_8](BF_4)_8 \cdot 16H_2O$ (**5**). Compound **1** crystallizes in the monoclinic system, space group $P2_1/c$, with $a = 14.937(1)$ Å, $b = 18.612(2)$ Å, $c = 20.583(2)$ Å, $\beta = 108.862(2)°$, $Z = 4$. Compound **2** crystallizes in the orthorhombic system, space group $P2_12_12$, with $a = 21.771(4)$ Å, $b = 13.700(2)$ Å, $c = 20.017(3)$ Å, $Z = 4$. Compound **3** crystallizes in the tetragonal system, space group $P4_3$, with $a = 12.9483(7)$ Å, $c = 33.416(3)$ Å, $Z = 4$. Compound **4** crystallizes in the triclinic system, space group $P\bar{1}$, with $a = 12.6677(8)$ Å, $b = 18.110(1)$ Å, $c = 19.998(1)$ Å, $\alpha = 100.395(1)°$, $\beta = 109.514(1)°$, $\gamma = 109.686(1)°$, $Z = 2$. Compound **5** crystallizes in the monoclinic system, space group $P2_1/n$, with $a = 21.153(5)$ Å, $b = 35.778(9)$ Å, $c = 21.823(5)$ Å, $\beta = 97.757(6)°$, $Z = 4$. The linear trinuclear Ni(II) complex (**2**) has a *cis*-N–N single bond bridge, and a water bridge linking the central Ni(II) to each external Ni(II) center in each of two similar trinuclear subunits, and exhibits intramolecular ferromagnetic exchange ($J = 5.0$ cm^{-1}). A novel octanuclear metallacyclic ring structure exists in **5**, with *trans*-N–N single bond bridges linking adjacent Ni(II) centers, leading to quite strong intramolecular antiferromagnetic exchange ($J = -30.4$ cm^{-1}).

Introduction

Open chain N−N single bond diazine based ligands have formed the basis for a number of useful studies relating magnetic properties to structural features associated with the rotationally flexible N−N bridge. Ditopic ligands such as PAHAP (Chart 1) form dinuclear μ(N−N) bridged complexes readily, and the N−N single bond bridge has proven to be very versatile in its ability to propagate exchange coupling between metal ion centers (e.g., Cu(II)), with a broad spectrum of exchange situations ranging from ferromagnetic at small M−N−N−M torsion angles ($<\sim 80°$) to antiferromagnetic at larger torsion angles.[1−6] The linear relationship between the rotational angle of the copper magnetic planes around the N−N bond and the exchange integral observed experimentally was supported by molecular orbital (extended Hückel) calculations, and related to the degree of overlap of the nitrogen p orbitals in the N−N bridge.[1,2] Dinuclear Ni(II) examples with similar ligands involving three N−N bridges between metal centers are very weakly antiferromagnetically coupled ($-2J < 1$ cm^{-1}), with Ni−N−N−Ni torsional angles in the range 39.8−42.8°.[6] In an unusual linear Ni(II)$_3$ complex composed of a dinuclear

* Corresponding author. E-mail: lthomp@mun.ca. Fax: 709-737-3702.

(1) Xu, Z.; Thompson, L. K.; Miller, D. O. *Inorg. Chem.* **1997**, *36*, 3985.
(2) Thompson, L. K.; Xu, Z.; Goeta, A. E.; Howard, J. A. K.; Clase, H. J.; Miller, D. O. *Inorg. Chem.* **1998**, *37*, 3217
(3) Xu, Z.; Thompson, L. K.; Miller, D. O.; Clase, H. J.; Howard, J. A. K.; Goeta, A. E. *Inorg. Chem.* **1998**, *37*, 3620.
(4) Xu, Z.; Thompson, L. K.; Matthews, C. J.; Miller, D. O.; Goeta, A. E.; Wilson, C.; Howard, J. A. K.; Ohba, M.; Okawa, H. *J. Chem. Soc., Dalton Trans.* **2000**, 69.
(5) Xu, Z.; White, S.; Thompson, L. K.; Miller, D. O.; Ohba, M.; Ōkawa, H.; Wilson, C.; Howard, J. A. K. *J. Chem. Soc., Dalton Trans.* **2000**, 1751.
(6) Xu, Z.; Thompson, L. K.; Black, D. A.; Ralph, C.; Miller, D. O.; Leech, M.; Howard, J. A. K. *J. Chem. Soc., Dalton Trans.* **2001**, 2042.

10.1021/ic0206950 CCC: $25.00
Published on Web 04/04/2003

Chart 1

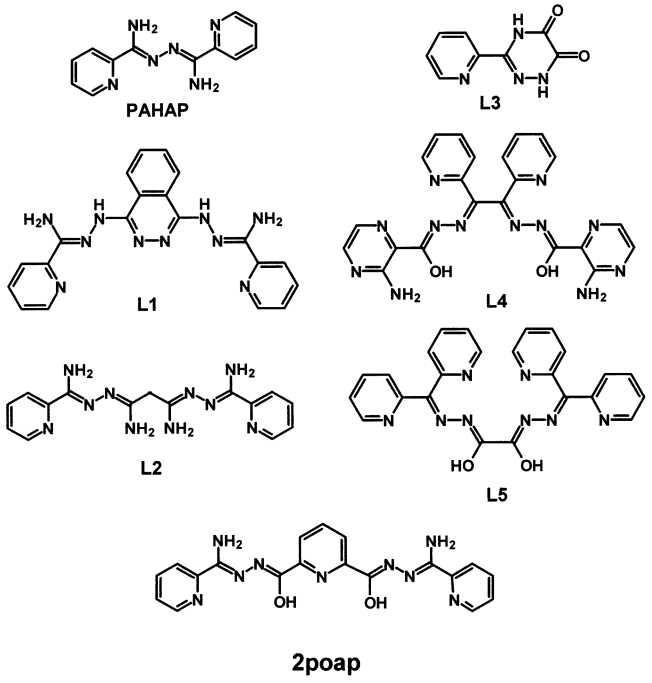

pyridazine (heterocyclic N−N) bridged site, and an isolated mononuclear site, somewhat stronger antiferromagentic exchange was observed ($-2J = 4.6$ cm^{-1}).[7]

The incorporation of N−N based bridging groups into more complex polytopic ligands creates a framework for the construction of larger, supramolecular, polynuclear systems, via self-assembly reactions, with built-in magnetically active subunits. This type of ligand has therefore been expanded to include a number of new polyfunctional diazine systems (Chart 1), by reactions involving, e.g., condensations of hydrazones and hydrazides with imino-picolinic acid methyl ester, and ethyl chloro-oxoacetate. The presence of several donor pockets in these ligands leads to the formation of larger polynuclear cluster complexes via self-assembly reactions. Ligands such as 2poap are of particular interest in this regard since they self-assemble in high yield in the presence of Mn(II), Fe(II), Cu(II), and Zn(II) salts to form novel [$M_9(\mu$-$O)_{12}$] [3 × 3] square grid complexes.[8−12] The complexes $[(L1)_2Ni_2(H_2O)_2](NO_3)_4\cdot 3H_2O$ (**1**), $[(L2)_2Ni_3(H_2O)_2](NO_3)_6\cdot 8H_2O$ (**2**), $[(L3)_4Ni_4(H_2O)_8](NO_3)_4\cdot 8H_2O$ (**3**), $[(L4)_2Ni_5(H_2O)_{10}(NO_3)](NO_3)_7\cdot 8H_2O$ (**4**), $(L5)_4Ni_8(H_2O)_8](BF_4)_8\cdot 16H_2O$ (**5**), and $[(L5)_4Ni_8(H_2O)_8](ClO_4)_8\cdot 4H_2O$ (**6**) are formed in high yield on reaction between the ligands L1−L5 and nickel(II) salts. Structural and magnetic properties of the complexes will be discussed.

Experimental Section

Physical Measurements. Infrared spectra were recorded as Nujol mulls using a Mattson Polaris FT-IR instrument, and UV−vis spectra were obtained as Nujol mulls with a Cary 5E spectrometer. Mass spectra were obtained with a VG Micromass 7070HS spectrometer, and microanalyses were carried out by Canadian Microanalytical Service, Delta, Canada. Variable temperature magnetic data (2−300 K) were obtained using a Quantum Design MPMS5S SQUID magnetometer with field strengths in the range 0.1−5.0 T. Samples were prepared in aluminum pans or gel caps, and background corrections for the sample holder assembly and diamagnetic components of the complex were applied.

Synthesis of the Ligands. L1. DHPH[13] (19.0 g, 0.1 mol) was suspended in a methanolic solution (100 mL) of methyl iminopicolinic ester (0.2 mol) generated by the reaction of 2-cyanopyridine (20.8 g, 0.2 mol) and sodium methoxide (20 mmol) in dry methanol, and the mixture refluxed for 5 h. The yellow precipitate formed was filtered off, washed with methanol and ether, and air-dried (yield 37 g; 93%). Mp 210−212 °C; IR $_{max}$/cm^{-1} (Nujol) 3467, 3383, 3338 (ν NH_2), 1656, 1616 (ν C═N) and 997 (py); mass spectrum (*m*/*z*) 399 (MH^+), 384, 281, 265, 200.

L2. Malonic dinitrile (13.2 g, 0.2 mol; Aldrich, purified before use) was added to a solution of absolute ethanol (20.0 g, 0.43 mol) and anhydrous diethyl ether (30 mL) in a round-bottom flask. The solution was stirred and maintained between −35 and −15 °C. Dry hydrogen chloride gas was bubbled into the reaction mixture until 22 g of HCl was absorbed. The reaction flask was stoppered tightly and allowed to stand in a freezer for 2 days. After removing solvent under vacuum, 42.3 g (91.6%) of the white solid intermediate product ethyl malonic diimidate hydrochloride was obtained, which was stored in a desiccator over sodium hydroxide/phosphorus pentoxide.

A cold solution of picolinamide hydrazone[14] (6.8 g, 0.05 mol in 50 mL dry methanol) was added to a cold solution (5 °C) of ethyl malonicdiimidate hydrochloride (5.8 g, 0.025 mol) in dry methanol (50 mL). The mixture was stirred at 5 °C for 30 min and then neutralized with saturated aqueous potassium bicarbonate solution. A light yellow solid precipitated, which was filtered off and washed with cold water, followed by small amounts of methanol and then diethyl ether (yield 6.61 g (78%)). Mp 115−117 °C; IR ν_{max}/cm^{-1} (Nujol) 3348, 3186 (NH_2), 1687, 1640 (C═N) and 998 (py); mass spectrum (*m*/*z*) 304 ($M - 2NH_3$), 275, 247, 198, 160, 105.

L3. Ethyl chloro-oxoacetate (13.6 g, 0.1 mol) dissolved in CH_2Cl_2 (50 mL) was added dropwise at −5 to 0 °C over a period of 1 h to a solution of picolinamide hydrazone[14] (15.0 g, 0.11 mol) dissolved in CH_2Cl_2 (100 mL). Triethylamine (11.0 g, 0.11 mol) was added slowly, and the solution refluxed for 2 h. Addition of the solution to water (100 mL) produced a light yellow solid, which was filtered off, washed with methanol and ether, and air-dried (yield 14.8 g, 78%). Mp 150−250 °C (broad); IR ν_{max}/cm^{-1} (Nujol) 3302, 3269 (OH, NH), 1701 (C═O), 997 (py); mass spectrum (*m*/*z*) 190 (M), 167, 154, 111.

L4. 3-Aminopyrazine-2-carboxylic acid hydrazide (0.78 g, 5.1 mmol) was reacted with dipyridyl diketone (0.55 g, 2.9 mmol) in refluxing absolute ethanol over 6 h. On cooling, a yellow precipitate formed, which was filtered off, washed with ethanol and ether, and air-dried (yield 1.05 g, 85%). Mp > 260 °C dec; IR ν_{max}/cm^{-1} (Nujol) 3302, 3269 (OH, NH), 1701 (C═O), 997 (py).

(7) Thompson, L. K.; Matthews, C. L.; Zhao, L.; Wilson, C.; Leech, M. A.; Howard, J. A. K. *J. Chem. Soc., Dalton Trans.* **2001**, 2258.
(8) Zhao, L.; Matthews, C. J.; Thompson, L. K.; Heath, S. L. *J. Chem. Soc., Chem. Commun.* **2000**, 265.
(9) Zhao, L.; Xu, Z.; Thompson, L. K.; Heath, S. L.; Miller, D. O.; Ohba, M. *Angew. Chem., Int. Ed.* **2000**, *39*, 3114.
(10) Waldmann, O.; Koch, R.; Schromm, S.; Müller, P.; Zhao, L.; Thompson, L. K. *Chem. Phys. Lett.* **2000**, *332*, 73.
(11) Waldmann, O.; Zhao, L.; Thompson, L. K. *Phys. Rev. Lett.* **2002**, *88*, 066401.
(12) Zhao, L.; Xu, Z.; Thompson, L. K.; Miller, D. O. *Polyhedron*, **2001**, *20*, 1359.
(13) Reynolds, G. A.; VanAllan, J. A.; Tinker, J. F. *J. Org. Chem.* **1959**, *24*, 1205.
(14) Case, F. H. *J. Org. Chem.* **1965**, *30*, 931.

Table 1. Summary of Crystallographic Data for **1**−**5**

	1	2	3	4	5
empirical formula	$C_{41}H_{52}N_{24}O_{19}Ni_2$	$C_{30}H_{59}N_{26}O_{29.5}Ni_3$	$C_{32}H_{53}N_{20}O_{36.5}Ni_4$	$C_{44}H_{71.5}N_{31}O_{44.25}Ni_5$	$C_{96}H_{110}N_{32}O_{31}B_4F_{16}Ni_8$
fw	1302.41	1432.05	1536.68	2036.23	3024.94
space group	$P2_1/c$ (No. 14)	$P2_12_12$ (No. 18)	$P4_3$ (No. 78)	$P\bar{1}$	$P2_1/n$ (No. 14)
a (Å)	14.937(1)	21.771(4)	12.9483(7)	12.6677(8)	21.153(5)
b (Å)	18.61292)	13.700(2)		18.110(1)	35.778(9)
c (Å)	20.583(2)	20.017(3)	33.416(3)	19.998(1)	21.823(5)
α (deg)	90	90	90	100.395(1)	90
β (deg)	108.862(2)	90	90	109.514(1)	97.757(6)
γ (deg)	90	90	90	109.686(1)	90
V (Å^3)	5414.9(7)	5960(1)	5602.4(5)	3843.3(4)	16365(6)
ρ_{calcd} (g cm^{-3})	1.597	1.593	1.822	1.759	1.228
Z	4	4	4	2	4
μ (cm^{-1})	7.93	10.43	14.47	13.24	9.83
λ (Å)	0.71073	0.71073	0.71073	0.71073	0.71073
T (K)	193(1)	193(1)	193(1)	193(1)	193(1)
R1[a]	0.045	0.084	0.048	0.053	0.14
wR2	0.110	0.251	0.135	0.145	0.446

[a] $R1 = \sum||2F_o| - |F_c|/\sum|F_o|$, $wR2 = [\sum[w(|F_o|^2 - |F_c|^2)^2]/\sum[w(|F_o|^2)^2]]^{1/2}$.

L5. Oxalic dihydrazide (1.18 g, 10 mmol) was added to a solution of dipyridyl ketone (3.68 g, 20 mmol) in methanol (100 mL), and the mixture refluxed for 10 h. A yellow solid formed, which was filtered off, washed with methanol and ether, and vacuum-dried (yield 3.4 g, 75%). Mp >270 °C dec. Mass spectrum (M/z) 451 (MH+), 226, 225, 197, 169, 105, 78. IR ν_{max}/cm^{-1} (Nujol) 1692 (CO), 1580, 1564 (CN), 997 (pyr). Anal. Calcd. For $C_{24}H_{18}N_8O_2$: C, 63.98; H, 4.03; N, 24.89; Found: C, 63.69; H, 3.96; N, 24.97.

Synthesis of the Complexes. $[(L1)_2Ni_2(H_2O)_2](NO_3)_4\cdot 3H_2O$ (1). L1 (0.4 g; 1.0 mmol) was reacted with $Ni(NO_3)_2\cdot 6H_2O$ (0.60 g; 2.1 mmol) in methanol/water (50/50; 20 mL) with warming. Large green crystals suitable for X-ray structural determination formed on prolonged standing at room temperature (yield 0.41 g, 80%). IR (ν cm^{-1}) (Nujol) 3240 (NH), 1687, 1657, 1585 (CN), 1013, 1023 (py); UV−vis (λ_{max} nm) 397, 500 (sh). 830. Anal. Calcd for $[(C_{20}H_{18}N_{10})_2Ni_2(H_2O)_2](NO_3)_4\cdot 3H_2O$: C, 38.42; H, 3.55; N, 26.89. Found: C, 38.37; H, 3.16; N, 27.14.

$[(L2)_2Ni_3(H_2O)_2](NO_3)_6\cdot 8H_2O$ (2). Ligand L2 (0.34 g, 1.0 mmol) was added to a solution of $Ni(NO_3)_2\cdot 6H_2O$ (0.87 g, 3.0 mmol) in a solvent mixture of 10 mL of H_2O and 5 mL of methanol. The mixture was stirred for a few minutes at room temperature and the resulting clear solution filtered. Deep green crystals suitable for X-ray diffraction formed from the filtrate after standing for several days at room temperature (yield: 75.8% based on the ligand). IR (ν cm^{-1}) (Nujol) 3324 (w) (H_2O and NH_2); 3164 (w, NH_2); 1659, 1631 (C═N); 1024 (m) (py); UV−vis (λ_{max} nm) 435, 590, 820, 1040. Anal. Calcd for $Ni_3(C_{15}H_{18}N_{10})_2(NO_3)_6(H_2O)_{10}$: C, 25.65; H, 4.02; N, 25.92. Found: C, 25.62; H, 3.82; N, 25.66.

$[(L3)_4Ni_4(H_2O)_8](NO_3)_4\cdot 8H_2O$ (3). L3 (0.19 g; 1.0 mmol) was added to a methanol/water (5 mL/10 mL) solution of $Ni(NO_3)_2\cdot 6H_2O$ (0.87 g, 3.0 mmol) with warming to form a green solution. Very large deep green crystals formed on standing, suitable for X-ray structural analysis (yield 0.29 g, 76%). IR (ν cm^{-1}) (Nujol) 3654, 3536 (H_2O), 1665 (C═O), 1025 (py); UV−vis (λ_{max} nm) 390, 634, 996. Anal. Calcd. for $Ni_4(C_8H_5N_5O_2)_4(NO_3)_4(H_2O)_{16}$: C, 25.16; H, 3.43; N, 18.34. Found: C, 24.98; H, 3.05; N, 18.34.

$[(L4)_2Ni_5(H_2O)_{10}(NO_3)](NO_3)_7\cdot 8H_2O$ (4). L4 (0.48 g; 1.0 mmol) was added to a solution of $Ni(NO_3)_2\cdot 6H_2O$ (0.87 g, 3.0 mmol) in methanol/water (20 mL/20 mL) and the mixture warmed forming a dark khaki-brown solution. Red-brown prismatic crystals of **4**, suitable for X-ray structural analysis, formed on standing (yield 0.73 g; 70%). IR (ν cm^{-1}) (Nujol) 3653, 3536 (coordinated H_2O), 3255 (NH), 1665 (C═O), 1025 (py); UV−vis (λ_{max} nm) 426, 558 (sh), 860, 1000. Anal. Calcd for $Ni_5(C_{22}H_{16}N_{12}O_2)_2(NO_3)_8(H_2O)_{18}$: C, 25.45; H, 3.40; N, 21.58. Found: C, 25.30; H, 3.05; N, 21.61.

$[(L5)_4Ni_8(H_2O)_8](BF_4)_8\cdot 16H_2O$ (5). L5 (0.050 g, 0.11 mmol) was added to a solution of $Ni(BF_4)_2\cdot 6H_2O$ (0.24 g, 0.71 mmol) in 2-propanol/water (15 mL/1 mL) and the mixture heated for 10 min forming a brown solution. The solution was filtered and placed in a desiccator containing wax flakes. Large brown rectangular plates suitable for X-ray structural analysis formed over a period of one month (yield 80%). IR ν_{max}/cm^{-1} (Nujol) 3455 (H_2O), 1627 (sh), 1568 (C═O, C═N), 1062 (BF_4); UV−vis (λ_{max} nm) 441, 561 (sh), 760, 819. Anal. Calcd for $Ni_8(C_{24}H_{16}N_8O_2)_4(BF_4)_8(H_2O)_{24}$: C, 33.99; H, 3.30; N, 13.22. Found: C, 33.75; H, 2.95; N, 13.21. $[(L5)_4Ni_8(H_2O)_8](ClO_4)_8\cdot 4H_2O$ (**6**) was prepared from a water/methanol solvent mixture in a manner similar to **5** using $Ni(ClO_4)_2\cdot 6H_2O$. The brown solution of the complex deposited dark brown crystals of **6** suitable for crystallographic studies on standing at room temperature (yield 82%). Anal. Calcd for $Ni_8(C_{24}H_{16}N_8O_2)_4(ClO_4)_8(H_2O)_{12}$: C, 35.21; H, 2.71; N, 13.69. Found: C, 35.12; H, 2.48; N, 13.77.

Crystallographic Data and Refinement of the Structures. The diffraction intensities of a pale green block-shaped crystal of **1** were collected with graphite monochromatized Mo Kα X-radiation (rotating anode generator) using a Bruker P4/CCD diffractometer at 193(1) K to a maximum 2θ value of 52.8°. The data were corrected for Lorentz and polarization effects. The structure was solved by direct methods.[15,16] All atoms except hydrogen atoms were refined anisotropically. Hydrogen atoms were introduced in difference map positions with isotropic thermal parameters set to 20% greater than their bonded partners at the time of their inclusion. They were all optimized by positional refinement, but the hydrogen atoms of the lattice water molecules were fixed for the final round of refinement. Neutral atom scattering factors[17] and anomalous-dispersion terms[18,19] were taken from the usual sources. All other calculations were performed with the teXsan[20] crystallographic software package using a PC computer. Data collections and

(15) (a) Sheldrick, G. M. *SHELX97*; 1997. (b) Altomare, A.; Cascarano, M.; Giacovazzo, C.; Guagliardi, A. SIR97. *J. Appl. Crystallgr*. **1993**, *26*, 343.
(16) DIRDIF94: Beurskens, P. T.; Admiraal, G.; Beurskens, G.; Bosman, W. P.; de Gelder, R.; Israel, R.; Smits, J. M. M. *The DIRDIF-94 program system*; Technical Report of the Crystallography Laboratory; University of Nijmegen: Nijmegen, The Netherlands, 1994.
(17) Cromer, D. T.; Waber, J. T. *International Tables for X-ray Crystallography*; The Kynoch Press: Birmingham, England, 1974; Vol. IV, Table 2.2 A.
(18) Ibers, J. A.; Hamilton, W. C. *Acta Crystallogr*. **1964**, *17*, 781.
(19) Creagh, D. C.; McAuley, W. J. *International Tables for Crystallography*; Wilson, A. J. C., Ed.; Kluwer Academic Publishers: Boston, 1992; Vol. C, Table 4.2.6.8, pp 219−222.

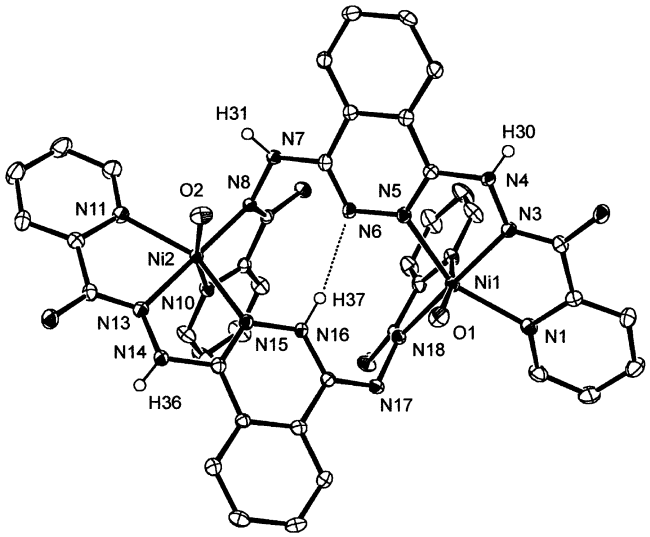

Figure 1. Structural representation of the cation in $[(L1)_2Ni_2(H_2O)_2](NO_3)_4 \cdot 3H_2O$ (**1**) (40% probability thermal ellipsoids).

Table 2. Selected Bond Distances (Å) and Angles (deg) for **1**

Ni(1)−O(1)	2.088(2)
Ni(1)−N(1)	2.131(3)
Ni(1)−N(3)	2.010(2)
Ni(1)−N(5)	2.081(2)
Ni(1)−N(18)	2.063(2)
Ni(1)−N(20)	2.094(2)
Ni(2)−O(2)	2.090(2)
Ni(2)−N(8)	2.005(2)
Ni(2)−N(10)	2.094(2)
Ni(2)−N(11)	2.119(3)
Ni(2)−N(13)	2.000(2)
Ni(2)−N(15)	2.117(2)
Ni(1)−Ni(2)	6.256(2)
N(16)−H(37)	0.923
H(37)−N(6)	2.239
N(16)−H(37)−N(6)	158.4
Ni(1)−N(5)−N(6)	123.07(16)
Ni(2)−N(15)−N(16)	125.37(16)

structural solutions for **1**−**5** were carried out in a similar manner. Abbreviated crystal data for **1**−**5** are given in Table 1. Crystallographic data are available as Supporting Information. Crystallographic data for **1**−**5** have also been deposited with the Cambridge Crystallographic Data Center, CCDC Nos. 202947−202951. Copies of this information may be obtained free of charge from The Director, CCDC, 12, Union Road, Cambridge, CB2 1EZ, U.K. (E-mail: deposit@ccdc.cam.ac.uk; http://www.ccdc.cam.ac.uk. Fax: +44−1223−336033.)

Results and Discussion

Structure of $[(L1)_2Ni_2(H_2O)_2](NO_3)_4 \cdot 3H_2O$ (1). The structural representation of the cation in **1** is shown in Figure 1, and relevant bond distances and angles are listed in Table 2. The dinuclear complex includes two neutral ligands and two octahedral NiN_5O nickel(II) centers, with each ligand acting in a twisted pentadentate manner and bridging the metals with a bidentate and a tridentate end. The central phthalazine subunits bond via one nitrogen only, unlike the situation involving the comparable Schiff base ligand PHP6Me, which forms 1:2 (ligand/metal) dinuclear complexes with Ni(II) and Co(II) with bridging diazine (N_2) and halogen atoms linking the metals together in close proximity (Ni−Ni 3.68 Å; Co−Co 3.71 Å).[21] In **1**, the Ni−Ni separation is very large (6.256 Å). Protons were located in difference maps on N(4), N(7), N(14), and N(16) (Figure 1) indicating that the two ligands are in different tautomeric forms in the same molecule. One ligand has two protonated exo-cyclic nitrogen atoms (N(4), N(7)), while the other has a proton on a ring nitrogen (N(16)), and an exocyclic nitrogen atom (N(14)). This leads to a hydrogen bonding situation involving the two phthalazine ring atoms N(6) and N(16) (N(16)−H(37) 2.24 Å; N(16)−H(37)−N(6) 158°), which effectively links the two rings together, and may prevent metal ion coordination at these sites.

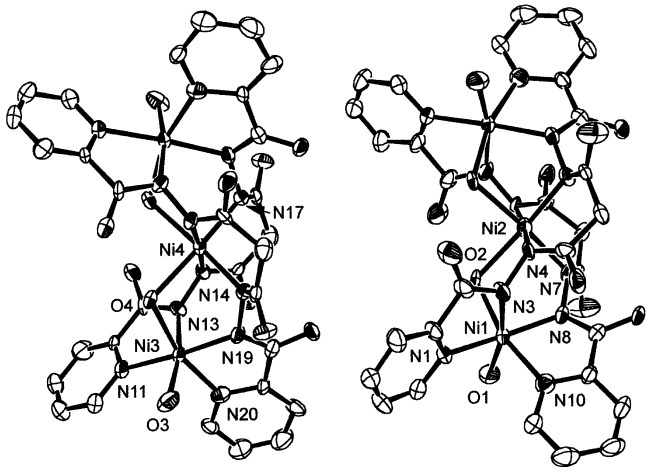

Figure 2. Structural representation of $[(L2)_2Ni_3(H_2O)_2](NO_3)_6 \cdot 8H_2O$ (**1**), showing the two trinuclear structures in the asymmetric unit (40% probability thermal ellipsoids).

Table 3. Selected Bond Distances (Å) and Angles (deg) for **2**

Ni(1)−O(1)	2.085(7)	Ni(1)−Ni(2)	3.409(2)
Ni(1)−O(2)	2.201(7)	Ni(1)−Ni(1)	6.581(2)
Ni(1)−N(1)	2.056(8)	Ni(3)−Ni(4)	3.433(2)
Ni(1)−N(3)	2.030(9)	Ni(3)−Ni(3)′	6.649(2)
Ni(1)−N(8)	2.044(8)	O(2)−O(12)′	2.650
Ni(1)−N(10)	2.057(8)	O(13)−N(18)	2.996
Ni(2)−O(2)	2.248(6)	Ni(3)−O(4)−Ni(4)	100.1(2)
Ni(2)−N(4)	2.076(8)		
Ni(2)−N(7)	2.073(8)		
N(3)−N(4)	1.440(12)		
Ni(3)−O(3)	2.051(7)		
Ni(3)−O(4)	2.218(7)		
Ni(3)−N(11)	2.096(8)		
Ni(3)−N(13)	2.029(8)		
Ni(3)−N(19)	2.027(8)		
Ni(3)−N(20)	2.053(7)		
Ni(4)−O(4)	2.260(7)		
Ni(4)−N(14)	2.084(7)		
Ni(4)−N(17)	2.070(8)		
N(13)−N(14)	1.423(11)		
N(17)−N(19)	1.480(9)		

Structure of $[(L2)_2Ni_3(H_2O)_2](NO_3)_6 \cdot 8H_2O$ (2). The molecular structure of **2** is illustrated in Figure 2, and important bond distances and angles are listed in Table 3. There are two slightly different trinuclear complex ions in the asymmetric unit each with three Ni(II) centers arranged in a linear fashion and with each pair of adjacent metal centers in each

(20) *teXsan for Windows: Crystal Structure Analysis Package*; Molecular Structure Corporation: The Woodlands, TX, 1997.

(21) Wen, T.; Thompson, L. K.; Lee, F. L.; Gabe, E. J. *Inorg. Chem.* **1988**, *27*, 4190.

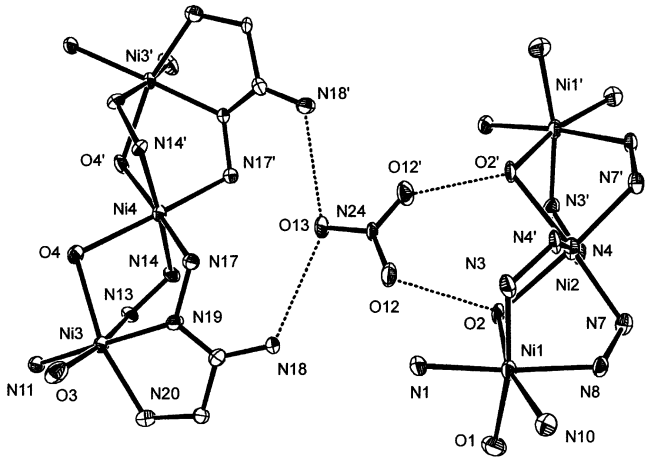

Figure 3. Extended structure for **2**, showing hydrogen bonding connections.

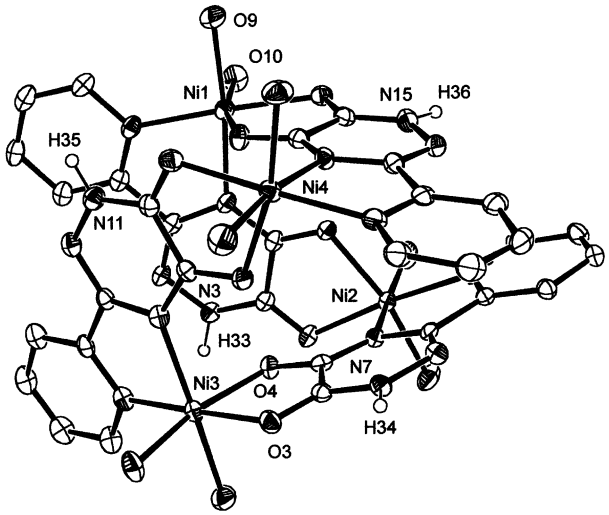

Figure 4. Structural representation of the tetranuclear cation in $[(L3)_4Ni_4(H_2O)_8](NO_3)_4 \cdot 8H_2O$ (**3**) (40% probability thermal ellipsoids).

trinuclear subunit bridged by two N−N diazine single bonds from separate ligands, and by a water molecule. Adjacent Ni−Ni separations are 3.409(2) Å (Ni(1)−Ni(2)) and 3.433(2) Å (Ni(3)−Ni(4)) in the two molcules, with distant Ni−Ni separations exceeding 6.58 Å. On the basis of the structure of the coordinated ligand (Chart 1), in which the C−N and N−N bond distances compare closely with those in the ligand picolinamide azine (PAHAP; Chart 1),[1] it is reasonable to assume that the ligand L2 is neutral and that the bridging oxygen atoms (O(2), O(4)) are water molecules (hydrogen atoms assigned to these centers were added in fixed positions). This is also supported by the presence of six nitrate groups and long Ni−O (H_2O) contacts (2.201−2.260 Å) typical of water in a bridging situation between two Ni(II) centers.[22−25] The Ni−O−Ni angles are 100.1(2)° (Ni(3), Ni(4)) and 100.0(3)° (Ni(1), Ni(2)), and N−N distances are quite long, falling in the range 1.424−1.480 Å, indicative of N−N single bonds. The *cis*-NiN_4O_2 centers have pseudo-octahedral geometries with Ni−N distances in the range 2.027−2.096 Å, and Ni−O distances in the range 2.051−2.260 Å, and are twisted around the N−N single bonds with very small Ni−N−N−Ni torsional angles between the symmetry related pairs of Ni atoms (Ni(1)−N(8)−N(7)−Ni(2) 27.0°; Ni(1)−N(3)−N(4)−Ni(2) 39.9°; Ni(3)−N(13)−N(14)−Ni(4) 41.5°; Ni(3)−N(19)−N(17)−Ni(4) 31.9°; av 35.1°). One terminal water molecule is bound to each Ni(II) center.

An examination of the extended structure of **2** reveals a network of contacts involving nitrate groups, the bridging water molecules, and NH_2 groups on the ligands. Nitrate N(24) (Figure 3) is positioned between the two molecules (a, b) with short contacts (2.650 Å) between O(12) and its symmetry related partner and the bridging waters (O(2), O(2)′), and a longer contact through O(13) to N(18) and N(18)′ (2.996 Å). A similar connection is found between O(4) and O(4)′ on molecule b to O(5) and O(5)′ (2.655 Å) of nitrate N(21), with a further long contact between nitrate oxygen O(6) and N(9) and N(9)′ (3.069 Å) on a. This series of contacts is considered significant in the magnetic analysis (vide infra).

Table 4. Selected Bond Distances (Å) and Angles (deg) for **3**

Ni(1)−O(10)	2.037(4)	Ni(4)−O(5)	2.086(5)
Ni(1)−O(9)	2.061(4)	Ni(4)−N(16)	2.093(5)
Ni(1)−N(1)	2.062(6)	Ni(1)−Ni(4)	5.432(2)
Ni(1)−O(8)	2.080(4)	Ni(1)−Ni(3)	6.654(2)
Ni(1)−N(4)	2.082(5)	Ni(2)−Ni(3)	5.417(2)
Ni(1)−O(7)	2.102(5)	Ni(2)−Ni(4)	6.565(2)
Ni(2)−O(11)	2.053(5)	Ni(1)−Ni(2)	5.444(2)
Ni(2)−O(12)	2.053(4)	Ni(3)−Ni(4)	5.404(2)
Ni(2)−O(2)	2.063(4)	Ni(4)−Ni(2)−Ni(1)	52.78(5)
Ni(2)−N(5)	2.067(5)	Ni(2)−Ni(1)−Ni(3)	52.04(5)
Ni(2)−N(8)	2.077(4)	Ni(1)−Ni(3)−Ni(4)	52.30(5)
Ni(2)−O(1)	2.088(5)	Ni(3)−Ni(4)−Ni(2)	52.74(5)
Ni(3)−N(9)	2.043(6)		
Ni(3)−O(13)	2.048(4)		
Ni(3)−O(4)	2.061(4)		
Ni(3)−O(14)	2.064(4)		
Ni(3)−N(12)	2.079(5)		
Ni(3)−O(3)	2.103(5)		
Ni(4)−O(15)	2.040(4)		
Ni(4)−O(6)	2.052(4)		
Ni(4)−O(16)	2.067(4)		
Ni(4)−N(13)	2.084(6)		

Structure of $[(L3)_4Ni_4(H_2O)_8](NO_3)_4 \cdot 8H_2O$ (3). The molecular structure of **3** is shown in Figure 4, and relevant bond distances and angles are listed in Table 4. The complex is a self-assembled tetrameric Ni_4L_4 entity, with the bridging triazine ligands acting in a tetradentate manner, binding through both oxygen atoms, and the pyridine and one triazine nitrogen atom. It is apparent that during the ligand synthesis ring closure occurred after the initial condensation reaction between the ethyl chloro-oxoacetate and picolinamide hydrazone, with the elimination of an ethanol molecule, and the formation of the triazine ring, rather than an open chain hydrazone derivative. Each nickel(II) center is bound simultaneously to N_2 and O_2 fragments from separate ligands, with two water molecules completing octahedral coordination. Protons H(33), H(34), H(35), and H(36) (Figure 4) were located in difference maps and occur on the nitrogen atoms at the 4-positions of the triazine rings. Each ligand loses one

(22) Cotton, F. A.; Winquist, B. H. C. *Inorg. Chem*. **1969**, *8*, 1304.
(23) McKenzie, E. D.; Stephens, F. S. *Inorg. Chim. Acta*, **1979**, *32*, 253.
(24) Ahlgrén, M.; Turpeinen, U.; Hämäläinen, R. *Acta Chem. Scand*. **1978**, *A32*, 189.
(25) Ahlgrén, M.; Turpeinen, U. *Acta Crystallogr*. **1982**, *B38*, 276.

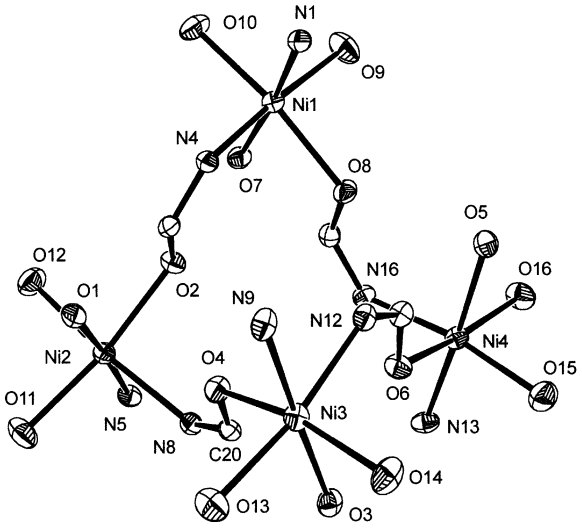

Figure 5. Structural representation of the tetranuclear core in **3** with atom labeling.

Chart 2

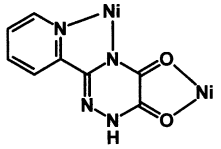

proton, and the location of these protons is consistent with the short CO distances (1.235−1.260 Å), and the significant double bond character of these bonds. Relatively long CN distances to the 1-nitrogen atoms (1.32−1.38 Å) are also consistent with this situation, indicating the 1-nitrogen to be the site of deprotonation, and the fact that the ligand is in the quinone tautomeric form (Chart 2). Carbonyl stretching in the infrared at 1665 cm^{-1} (vide ante) is consistent with this.

The Ni_4 cluster has a distorted, folded tetrahedral shape, with the four pseudo-octahedral NiN_2O_4 centers linked by NCO frameworks (Figure 5), with distances between adjacent nickel atoms in the range 5.40−5.45 Å. Ni−N and Ni−O distances fall in the ranges 2.043−2.093 and 2.037−2.103 Å, respectively, typical for Ni(II) ions in this sort of environment. The Ni−O (L3) distances are slightly larger than the Ni−O (H_2O) distances.

Structure of $[(L4)_2Ni_5(H_2O)_{10}(NO_3)](NO_3)_7\cdot 8H_2O$ (4). The molecular structure of the cation in **4** is illustrated in Figure 6, and relevant bond distances and angles are listed in Table 5. The cluster comprises two ligands and five pseudo-octahedral nickel(II) centers, with a well separated dinuclear and a trinuclear subunit. Each ligand pivots and rotates along the carbon−carbon bond connecting the two pyridine groups, forming a central 12-membered metallacyclic ring, incorporating Ni(1) and Ni(3). Ni(1) and Ni(4) are bridged directly by a diazine group (N(20)−N(21)) in the dinuclear subunit, while Ni(3) is bridged to Ni(2) by a diazine (N(8)−N(9)), and by an alkoxide (O(3)) in the trinuclear subunit. A variety of nickel chromophores are present including *cis*-NiN_4O_2 (Ni(1)), *mer*-NiN_3O_3 (Ni(2), Ni(4)), *fac*-NiN_3O_3 (Ni(3)), and $NiNO_5$ (Ni(5)), with one nitrate bound to Ni(5) via O(16), and the other oxygen sites occupied by

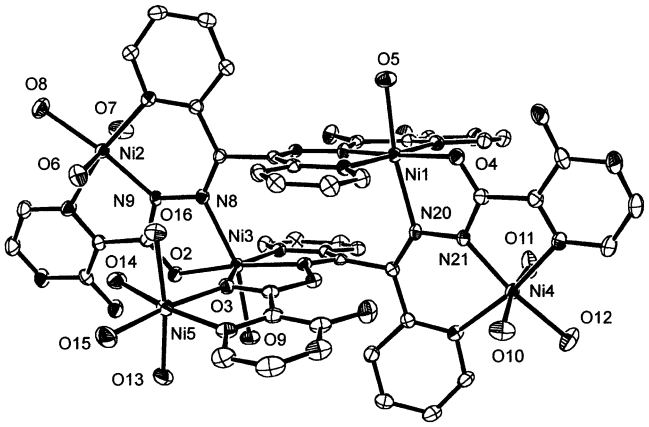

Figure 6. Structural representation of the pentanuclear cation in $[(L4)_2Ni_5(H_2O)_{10}(NO_3)](NO_3)_7\cdot 8H_2O$ (**4**) (40% probability thermal ellipsoids).

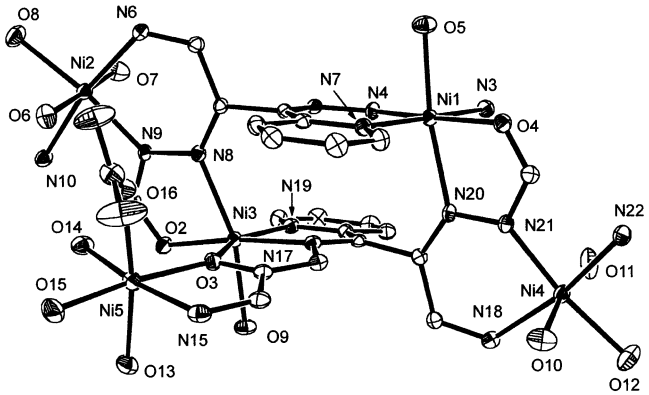

Figure 7. Structural representation of the pentanuclear core in **4**.

Table 5. Selected Bond Distances (Å) and Angles (deg) for **4**

Ni(1)−N(4)	1.961(3)	Ni(4)−N(21)	1.994(4)
Ni(1)−O(4)	2.002(3)	Ni(4)−O(12)	2.058(3)
Ni(1)−N(7)	2.031(4)	Ni(4)−O(11)	2.064(4)
Ni(1)−O(5)	2.089(3)	Ni(4)−O(10)	2.074(3)
Ni(1)−N(3)	2.132(4)	Ni(4)−N(18)	2.074(4)
Ni(1)−N(20)	2.174(3)	Ni(4)−N(22)	2.087(4)
Ni(2)−N(9)	1.989(3)	Ni(5)−O(14)	2.019(3)
Ni(2)−O(8)	2.059(3)	Ni(5)−O(13)	2.039(3)
Ni(2)−N(6)	2.063(4)	Ni(5)−N(15)	2.048(4)
Ni(2)−O(6)	2.075(3)	Ni(5)−O(15)	2.054(3)
Ni(2)−N(10)	2.080(4)	Ni(5)−O(3)	2.081(3)
Ni(2)−O(7)	2.093(4)	Ni(5)−O(16)	2.107(3)
Ni(3)−O(2)	2.002(3)	Ni(1)−Ni(4)	4.894(2)
Ni(3)−N(17)	2.012(3)	Ni(3)−Ni(5)	3.986(3)
Ni(3)−O(9)	2.071(3)	Ni(2)−Ni(3)	4.908(2)
Ni(3)−N(19)	2.075(4)	Ni(2)−Ni(5)	5.779(3)
Ni(3)−Ni(4)	7.607(3)	Ni(1)−Ni(3)	5.357(3)
Ni(3)−N(8)	2.145(3)	Ni(1)−Ni(2)	8.102(2)
Ni(3)−O(3)	2.200(3)	Ni(5)−O(3)-Ni(3)	137.17(15)

water molecules. A simplified view of the pentanuclear cluster is shown in Figure 7.

Within the trinuclear subunit, Ni(2) and Ni(3) are bridged by an almost *trans* diazine (N(8)−N(9) 1.374 Å) with a torsional (Ni−N−N−Ni; τ) angle of 137.2°. Ni(3) and Ni(5) are bridged by an asymmetric alkoxide linkage (Ni(3)−O(3) 2.200 Å; Ni(5)−O(3) 2.081 Å), with a large bridge angle (137.2°). In the dinuclear subunit, Ni(1) and Ni(4) are bridged by an almost *trans* N−N linkage (τ = 161.4°; N(20)−N(21) 1.375 Å). Ni(1)−Ni(4) (4.894 Å) and Ni(2)−Ni(3) (4.908 Å) distances are longer than the Ni(3)−Ni(5) (3.986 Å) distance, as would be expected. The separation

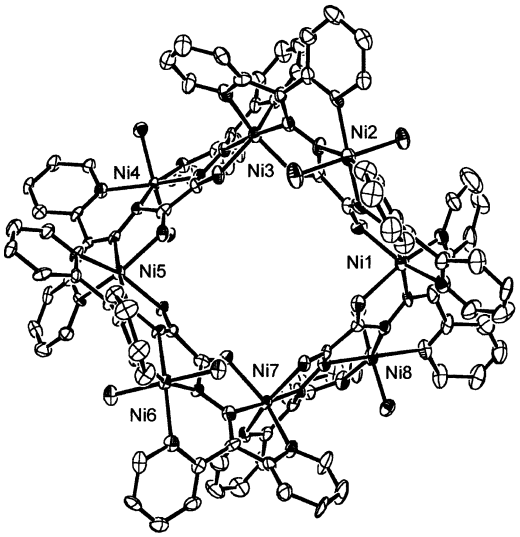

Figure 8. Structural representation of the octanuclear cation in $[(L5)_4Ni_8(H_2O)_8](BF_4)_8 \cdot 16H_2O$ (**5**) (35% probability thermal ellipsoids).

Table 6. Selected Bond Distances (Å) and Angles (deg) for **5**

Ni(1)−N(30)	1.943(13)	Ni(4)−O(12)	2.082(9)
Ni(1)−N(3)	1.985(14)	Ni(4)−O(11)	2.103(10)
Ni(1)−N(32)	2.029(14)	Ni(5)−N(19)	1.973(11)
Ni(1)−O(13)	2.106(10)	Ni(5)−N(14)	1.980(11)
Ni(1)−N(1)	2.106(13)	Ni(5)−N(16)	2.051(11)
Ni(1)−O(2)	2.119(10)	Ni(5)−O(10)	2.095(10)
Ni(2)−N(5)	2.012(13)	Ni(5)−N(17)	2.099(12)
Ni(2)−N(4)	2.027(14)	Ni(5)−O(3)	2.119(9)
Ni(2)−N(7)	2.065(13)	Ni(6)−N(21)	2.000(11)
Ni(2)−N(2)	2.089(14)	Ni(6)−N(20)	2.018(10)
Ni(2)−O(7)	2.098(12)	Ni(6)−N(18)	2.064(11)
Ni(2)−O(8)	2.101(11)	Ni(6)−O(5)	2.107(10)
Ni(3)−N(11)	1.955(12)	Ni(6)−O(6)	2.118(10)
Ni(3)−N(6)	1.976(13)	Ni(6)−N(23)	2.123(13)
Ni(3)−N(8)	2.025(15)	Ni(7)−N(22)	1.978(12)
Ni(3)−N(9)	2.090(14)	Ni(7)−N(27)	1.985(11)
Ni(3)−O(9)	2.103(11)	Ni(7)−N(25)	2.059(13)
Ni(3)−O(14)	2.138(10)	Ni(7)−N(24)	2.080(12)
Ni(4)−N(12)	2.016(12)	Ni(7)−O(1)	2.112(9)
Ni(4)−N(13)	2.021(11)	Ni(7)−O(4)	2.147(9)
Ni(4)−N(10)	2.040(12)	Ni(8)−N(29)	1.994(13)
Ni(4)−N(15)	2.061(12)	Ni(8)−N(28)	2.040(11)
Ni(8)−O(15)	2.070(12)	Ni(4)−Ni(5)	4.750(7)
Ni(8)−N(31)	2.071(14)	Ni(5)−Ni(6)	4.779(8)
Ni(8)−O(16)	2.100(11)	Ni(6)−Ni(7)	4.759(7)
Ni(8)−N(26)	2.105(12)	Ni(7)−Ni(8)	4.782(8)
Ni(1)−Ni(2)	4.788(8)	Ni(8)−Ni(1)	4.748(8)
Ni(2)−Ni(3)	4.740(7)	Ni−N−N−Ni	152.0−161.0
Ni(3)−Ni(4)	4.734(8)		

between Ni(1) and Ni(3) (5.357 Å), and the long bridging pathways (five and six bonds), indicates that the two halves of the cluster are well separated magnetically (vide infra). Ni−O and Ni−N distances are typical for systems of this type.

Structure of $[(L5)_4Ni_8(H_2O)_8](BF_4)_8 \cdot 16H_2O$ (5). The molecular structure of the octanuclear cation in **5** is illustrated in Figure 8, and relevant bond distances and angles are listed in Table 6. The refinement of the structure proceeded normally and clearly revealed the structural details of the cation, but a low reflection/parameter ratio leads to a marginal level of refinement. Only four BF_4 anions are clearly identified, and it is reasonable to assume that in agreement with the elemental analysis others are "hidden" within the large number of peaks assigned to water molecules. The octanuclear ring structure forms by what is clearly a self-assembly process, and the individual subunits (Chart 3) show that the ligand is decadentate and all the coordination pockets are occupied by Ni(II) centers, with water molecules completing axial coordination sites at Ni(a). Self-assembly occurs by association of the ends (Ni(b)) of each subunit into the octanuclear ring, thus creating two different nickel(II) chromophores (*cis*- and *trans*-NiN_4O_2) (Figure 9). Each adjacent pair of nickel atoms is bridged by a N−N single bond as the primary bridging subunit (N−N 1.32−1.37 Å), with Ni−N−N−Ni torsional angle in the range 155−161°. Ni−Ni distances fall in the range 4.73−4.79 Å. Ni−O and Ni−N distances are typical for systems of this sort.

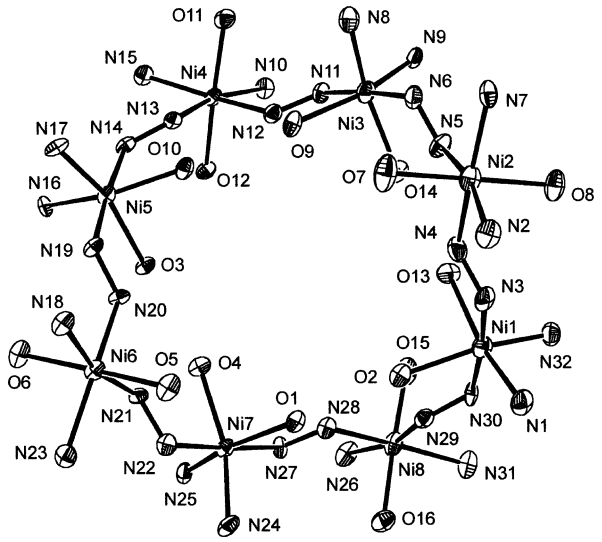

Figure 9. Structural representation of the octanuclear core in **5**.

Chart 3

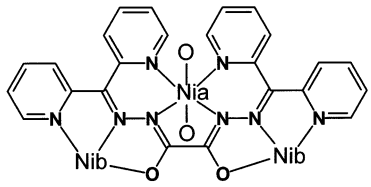

The ligands fold themselves around the outside of the Ni_8 ring and create a large hole with most of the oxygen atoms pointing inward. The hole has a diameter of 7−8 Å, and within the limits of the current refinement a cluster of three peaks assigned to oxygen atoms was located inside the hole, at reasonable hydrogen bonding distances. The overall ring cluster has a diameter of ∼20 Å, placing it well into the nanometer range. $[(L5)_4Ni_8(H_2O)_8](ClO_4)_8 \cdot 4H_2O$ (**6**) has an essentially identical Ni_8 ring structure but again suffers the problem of a marginal refinement.[26]

Magnetic Properties. The variable temperature magnetic data (μ_{mol}) for **1** are shown in Figure 10. The moment drops very slightly as temperature is lowered from room temper-

(26) Monoclinic, space group $P2_1/n$, M = 6562.4, a = 18.206(3) Å, b = 41.433(7) Å, c = 19.080(3) Å, β = 99.408°, Z = 2, R1 = 0.152, wR2 = 0.428.

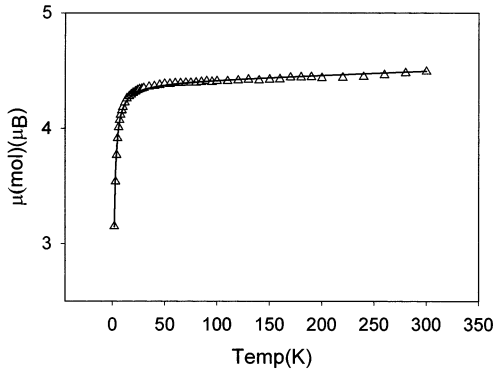

Figure 10. Variable temperature magnetic data for **1**. Solid line calculated from eq 1 with $g = 2.199(1)$, $J = -1.04(1)$ cm^{-1}, TIP $= 380 \times 10^{-6}$ emu·mol^{-1}, $\rho = 0$, $\theta = 0$ K ($10^2R = 0.59$).

ature down to about 25 K, and then, it drops more precipitously. This behavior suggests very weak intramolecular antiferromagnetic exchange, but the possible contribution of a zero field splitting component should also be considered. The data were fitted initially to a simple isotropic exchange model for two interacting $S = 1$ centers (eq 1).

$$H_{ex} = -J(S_1 \cdot S_2) \tag{1}$$

$$\chi_{M'} = \frac{N\beta^2 g^2}{3k(T-\theta)} \frac{\sum S_T(S_T+1)(2S_T+1)e^{-E(S_T)/kT}}{\sum (2S_T+1)e^{-E(S_T)/kT}} \tag{2}$$

$$\chi_M = \chi_{M'}(1-\rho) + \frac{4S(S+1)N\beta^2 g^2 \rho}{3kT} + \text{TIP} \tag{3}$$

The total spin state combinations, and their energies, were calculated using the Kambe approach[27] and substituted into the van Vleck equation (eq 2) to generate the appropriate exchange expression within the software of the MAGMUN4.0 magnetic package,[28] which deals conveniently with a wide variety of cluster models in a Windows based environment. Paramagnetic impurity fraction (ρ) and temperature independent paramagnetism (TIP) corrections are accounted for with eq 3. A good data fit was obtained for $g = 2.199(1)$, $J = -1.04(1)$ cm^{-1}, TIP $= 380 \times 10^{-6}$ emu·mol^{-1}, $\rho = 0$, $\theta = 0$, $10^2R = 0.59$ ($R = [(\chi_{obs} - \chi_{calc})^2/\chi_{obs}^2]^{1/2}$; θ = Weiss-like corrective term to account for weak intermolecular associations). The solid line in Figure 10 was calculated with these parameters. Introduction of a zero field splitting term also gave a reasonable fit with $g = 2.201(2)$, $J = -0.60(2)$, TIP $= 380 \times 10^{-6}$ emu·mol^{-1}, $\rho = 0$, $\theta = 0$, $D = -0.02$ cm^{-1} ($10^2R = 0.83$). We conclude that a weak antiferromagnetic exchange term is operating across the metallacyclic ring in **1**, over six bonds. The magnetic properties of **1** are in sharp contrast to those of dinuclear Ni(II) and Co(II) complexes of the related ligand PHP6Me, derived form the reaction of 1,4-dihydrazinophthalazine and 6-methyl-2-pyridine carboxaldehyde, in which the two metal ion centers are linked directly by the phthalazine (N−N) and chloro bridges.[21] J was found to be -26 cm^{-1} in the dinickel case.

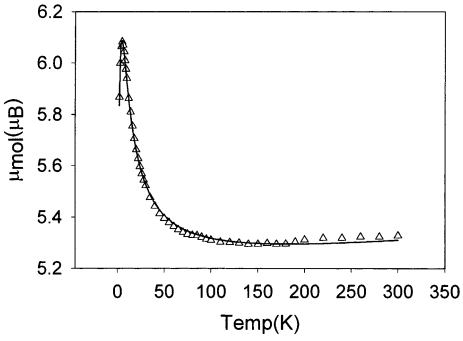

Figure 11. Variable temperature magnetic data for **2**. Solid line calculated from eq 5 with $g = 2.11(1)$, $J_1 = 5.0(1)$ cm^{-1}, $J_2 = -1.3$ cm^{-1}, TIP $= 450 \times 10^{-6}$ emu·mol^{-1}, $\rho = 0.003$, $\theta = -0.96$ K ($10^2R = 0.43$).

The variable temperature magnetic properties (μ_{mol}) of **2** are illustrated in Figure 11. The moment shows a gradual increase from a room temperature value of 5.3 μ_B to 6.08 μ_B at 4 K, followed by a slight drop at lower temperature. This behavior is typical of a system exhibiting dominant intramolecular ferromagnetic exchange coupling. Two exchange models were examined (eqs 4 and 5), one with just nearest neighbor exchange (eq 4), and another involving exchange between external Ni(II) centers as well (eq 5). The total spin state combinations, and their energies for both models, were calculated as before using the MAGMUN4.0 magnetic package.[28]

$$H_{ex} = -J\{S_1 \cdot S_2 + S_2 \cdot S_3\} \tag{4}$$

$$H_{ex} = -J_1\{S_1 \cdot S_2 + S_2 \cdot S_3\} - J_2\{S_1.S_3\} \tag{5}$$

The experimental data were fitted successfully to the magnetic model derived from eq 4 to give $g = 2.14(2)$, $J = 1.7(2)$ cm^{-1}, TIP $= 385 \times 10^{-6}$ emu·mol^{-1}, $\rho = 0.004$, $\theta = -1.1$ K ($10^2R = 1.5$). Fitting to eq 5 gave $g = 2.11(1)$, $J_1 = 5.0(1)$ cm^{-1}, $J_2 = -1.3(1)$ cm^{-1}, TIP $= 0.000450$ emu·mol^{-1}, $\rho = 0.003$, $\theta = -0.96$ K ($10^2R = 0.43$). The considerably improved fitting to eq 5 suggests that the negative J_2 value is significant, indicating a weak antiferromagnetic interaction between the external nickel centers within the same molecule, despite long distances of separation. The solid line in Figure 11 was calculated from the best-fit parameters using eq 5. The positive J (J_1) value in each case indicates the presence of dominant intramolecular ferromagnetic exchange between adjacent nickel(II) centers. The weak downturn of the magnetic data below 4 K could possibly be associated with zero field splitting effects, but it seems more likely due to intermolecular exchange effects associated with the extended structure shown in Figure 3. Magnetization data were obtained as a function of field at 2 K and show a rapid rise to $5.5N\beta$ at 5.0 T but did not reach complete saturation. This value approaches the theoretical value for a system with an $S = 3$ ground state, consistent with the other magnetic data.

(27) Kambe, K. *J. Phys. Soc. Jpn.* **1950**, *5*, 38.

(28) MAGMUN4.0 is available free of charge. It has been developed by Dr. Zhiqiang Xu (Memorial University) in collaboration with Prof. L. K. Thompson (lthomp@mun.ca), and Dr. O. Waldmann (waldmann@mps.ohio-state.edu), who wrote the energy state routine (Ow01.exe). We do not distribute the source codes. The programs may be used only for scientific purposes, and economic utilization is not allowed. If either routine is used to obtain scientific results, which are published, the origin of the programs should be quoted.

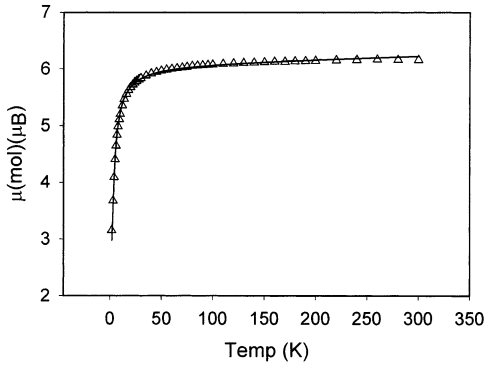

Figure 12. Variable temperature magnetic data for **3**. Solid line calculated from eq 6 with $g = 2.154(4)$, $J = -1.41(3)$ cm^{-1}, TIP $= 800 \times 10^{-6}$ emu·mol^{-1}, $\rho = 0.004$, $\theta = 0$ K ($10^2R = 1.07$).

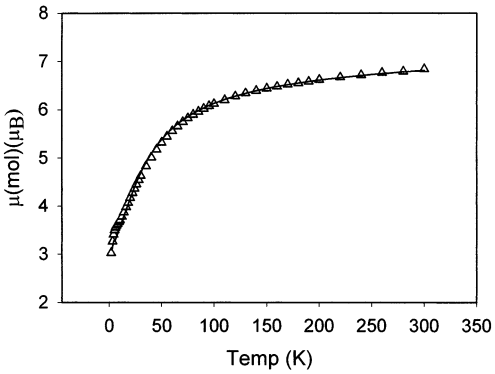

Figure 13. Variable temperature magnetic data for **4**. Solid line calculated from eq 7 with $g = 2.19(1)$, $J_1 = -50.0(5)$ cm^{-1}, $J_2 = -7.5$ cm^{-1}, TIP $= 1000 \times 10^{-6}$ emu·mol^{-1}, $\rho = 0.0005$, $\theta = 1.0$ K ($10^2R = 0.30$).

The magnetic properties of **2** can be interpreted in terms of the two different bridging groups (N−N, H_2O) and the geometrical consequences of the twisted bridging arrangement. The Ni−O−Ni bridge angles are large enough (>100°) that it is reasonable to assume that any exchange via this bridge is not likely to be ferromagnetic, and in fact, it might be expected to propagate a weak antiferromagnetic contribution based on the typical behavior of hydroxide bridged dinuclear, copper(II) compounds,[29] phenoxide bridged dinuclear nickel(II) complexes,[30] and an ab initio theoretical study on Ni−(μ-O)$_2$−Ni model compounds.[31] This being the case, the net ferromagnetic exchange can be considered to result from the N−N bridges only and dominates the overall exchange process. In the three previous cases involving three N−N bridges linking two Ni(II) centers,[6,7] with Ni−N−N−Ni torsional angles in the range 39.8−42.8°, weak antiferromagnetic exchange was observed. In the present case, the torsional angles are on average much lower. It is therefore reasonable to assume that, on the basis of the linear relationship between the copper magnetic plane angle (and by inference Cu−N−N−Cu torsional angle) with the exchange coupling in related copper(II) systems,[1−7] such small Ni−N−N−Ni angles would of necessity lead to ferromagnetic exchange. Compound **2** is therefore unique in this class, in that the diazine bridges are responsible for ferromagnetic coupling, and it joins $Ni_3(acac)_6$ as a rare example of a ferromagnetic trinuclear Ni(II) complex. It is perhaps of significance to note that the Ni−O−Ni bridge angles in $Ni_3(acac)_6$[32] fall in the range 76.5−89.3°, well into the ferromagnetic realm for typical M−O−M bridged systems.[29−31]

The variable temperature magnetic data (μ_{mol}) for **3** are shown in Figure 12, and the slight downward trend in the range 300−50 K, followed by a sharp drop to 2 K, is indicative of weak intramolecular antiferromagnetic exchange coupling. The data were fitted to a square exchange model, equivalent to the structural arrangement in **3**, based on a simple isotropic exchange Hamiltonian expression (eq 6) using MAGMUN4.0 to give $g = 2.154(4)$, $J = -1.41(3)$ cm^{-1}, $\rho = 0.004$, TIP $= 800 \times 10^{-6}$ emu·mol^{-1}, $\theta = 0$ K ($10^2R = 1.07$).

$$H_{ex} = -J\{S_1 \cdot S_2 + S_2 \cdot S_3 + S_3 \cdot S_4 + S_1 \cdot S_4\} \qquad (6)$$

The solid line in Figure 12 was calculated with these parameters. Introduction of a zero field splitting term did not change the fitting significantly, and an estimate of $D = -1$ cm^{-1} was obtained with a very slight change in J, indicating that the dominant effect is weak intramolecular antiferromagentic exchange. The four bond connections between adjacent pairs of nickel(II) centers are therefore considered responsible for this exchange interaction. The complexity of the structure of **4** suggests that an understanding of the exchange situation may be difficult. However, the pentanuclear cluster can conveniently be separated into two distinct and separate parts. In the dinuclear part, Ni(1) and Ni(4) are connected by a "trans" N−N diazine bridge. In the trinuclear part, a very similar N−N bridge connects Ni(2) and Ni(3), and Ni(3) and Ni(5) are connected by an alkoxide bridge. A secondary three atom (N−C−N) bridge connection also links Ni(1) and Ni(4) and Ni(2) and Ni(3) but is not considered significant in comparison with the direct N−N bridge. The magnetic structure of **4** was therefore considered as the simple sum of a dinuclear and a trinuclear exchange expression (Hamiltonian; eq 7), and because of the similarity between the N−N bridges only two exchange terms are used (J1 for the alkoxide bridge, and J2 for the diazine bridges).

$$H_{ex} = [-J_1\{S_5 \cdot S_3\} - J_2\{S_2 \cdot S_3\}] - [J_2\{S_1 \cdot S_4\}] \qquad (7)$$

The variable temperature magnetic data (μ_{mol}) are shown in Figure 13, with a pronounced drop in total moment as temperature is lowered consistent with significant intramolecular antiferromagnetic exchange. The data were fitted successfully to eq 7 via MAGMUN4.0 to give $g = 2.19(1)$, $J_1 = -50.0(5)$ cm^{-1}, $J_2 = -7.5$ cm^{-1}, $\rho = 0.0005$, TIP $= 1000 \times 10^{-6}$ emu·mol^{-1}, $\theta = 1.0$ K ($10^2R = 0.30$). The solid line in Figure 13 was calculated with these parameters. No attempt was made to include any zero field splitting terms. The large $-J_1$ value is consistent with an alkoxide bridged Ni(II) pair with a large Ni−O−Ni angle,[29,30] and

(29) Crawford, V. H.; Richardson, H. W.; Wasson, J. R.; Hodgson, D, J.; Hatfield, W. E. *Inorg. Chem.* **1976**, *15*, 2107.
(30) Nanda, K. K.; Thompson, L. K.; Bridson, J. N.; Nag, K. *J. Chem. Soc., Chem. Commun.* **1994**, 1337.
(31) Wang, C.; Fink, K.; Staemmler, V. *Chem. Phys.* **1995**, *192*, 25.
(32) Ginsberg, A. P.; Martin, R. L.; Sherwood, R. C. *Inorg. Chem.* **1968**, *7*, 932.

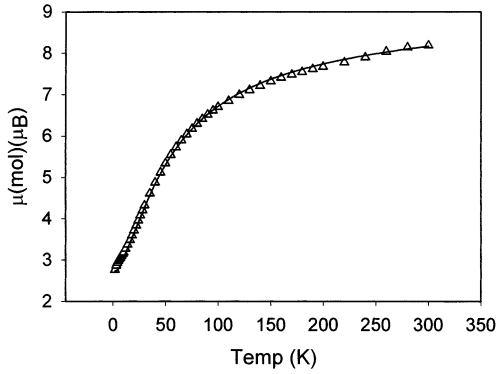

Figure 14. Variable temperature magnetic data for **5**. Solid line calculated from eq 8 with $g = 2.16(1)$, $J = -30.4(6)$ cm^{-1}, TIP $= 1600 \times 10^{-6}$ emu·mol^{-1}, $\rho = 0.10$, $\theta = 0$ K ($10^2R = 2.20$).

the assignment of J_2 to the almost *trans* diazine bridged Ni(II) pairs is also reasonable.[6,7]

The variable temperature magnetic data for **5** (μ_{mol}) show a sharp drop in moment from 8.3 μ_B at 300 K to 2.8 μ_B at 2 K (Figure 14), indicative of quite strong intramolecular antiferromagnetic exchange. A very similar profile was observed for **6**. The structure shows that within the ring of eight Ni(II) centers the metal ions are connected by eight N−N single bond bridges as the fundamental magnetic linkage, and that the geometry at each N−N bridge is very similar (Ni−N−N−Ni torsional angles 152−161°). The data were therefore fitted to an exchange expression for eight $S = 1$ spin centers arranged in a ring with a single J value, based on the appropriate exchange Hamiltonian (eqn. 8), using MAGMUN4.0.

$$H_{ex} = -J\{S_1 \cdot S_2 + S_2 \cdot S_3 + S_3 \cdot S_4 + S_4 \cdot S_5 + S_5 \cdot S_6 + S_6 \cdot S_7 + S_7 \cdot S_8 + S_1 \cdot S_8\} \quad (8)$$

A good fit was obtained for $g = 2.16(1)$, $J = -30.4(6)$ cm^{-1}, $\rho = 0.10$, $\theta = 0$, TIP $= 1600 \times 10^{-6}$ emu·mol^{-1} ($10^2R = 2.2$). The solid line in Figure 14 was calculated with these parameters. An excellent fit for **6** gave $g = 2.220(3)$, $J = -28.8(2)$ cm^{-1}, $\rho = 0.05$, $\theta = 0$, TIP $= 1600 \times 10^{-6}$ emu·mol^{-1} ($10^2R = 0.51$). The $-J$ values for **5** and **6** are quite large, indicative of efficient exchange within the Ni_8 ring, and somewhat larger than the comparable value found for **4**, but consistent with the *trans* arrangement of the Ni(II) centers relative to the N−N bridge.[6,7] Significant paramagnetic impurity corrections were required in both data analyses and may reflect a small proportion of incompletely metalated rings present in the bulk sample.

Compounds **5** and **6** bear a resemblance to cyclic Mn(III)$_6$ complexes of formyl- and acetyl-salicylhydrazide, which self-assemble with N−N single bond bridges as the main intermetallic connection. Magnetic exchange in these systems was not discussed.[33,34] Other examples in this class of rare self-assembled rings include Cr(III)$_8$[35] and Cr(III)$_{10}$[36] carboxylates, derived from basic chromium actetate, and even larger rings, e.g., Ni(II)$_{24}$,[37] derived from ligands such as 3-methyl-3-pyrazolin-5-one.

Conclusion

The design of polytopic ligands with a predictable outcome in a self-assembly process is fraught with limitations based on a number of factors, including the topological complexity of the ligand itself, but also because individual coordinating components in the ligands do not always behave in a manner similar to their single ligand counterparts. One over-riding feature that helps to create self-assembled clusters is the presence of ligand pockets that form five-membered chelate rings. This helps to prevent the ligand chelating to a single metal ion center and forces it to look for additional Lewis acid species. The linear tritopic ligand 2poap (Chart 1), and its derivatives, are classic examples where linear arrangements of coordination pockets allow trinuclear subunits to interlock in a high yield self-assembly process to yield nonanuclear grids.

Of the ligands L1−L5, only L3 and L5 show a perhaps predictable self-assembly outcome, based of course on the retrospective structural results. The primary coordination of adjacent pyridine and triazine nitrogens in L3 to a single nickel center creates an essentially flat subunit, which coordinates further by using the dihydroxy fragment to chelate to a second nickel center in a *cis*-fashion, with a distorted tetrahedron as the outcome. L5 has three coordination pockets (Chart 3), and the meridional coordination to Ni(b) creates a good opportunity for self-assembly to occur; this occurs neatly to generate the Ni_8 ring by both ends of the subunit joining up, in what is a geometrically favorable arrangement. In essence, in this case the self-assembly involves a polynuclear subunit and, so, highlights a possibly useful strategy for generating even larger clusters. Efforts are underway to create larger polytopic ligands of this type, with very large clusters as the ultimate target, and to explore further the coordination chemistry of L1−L5 and related ligands.

Acknowledgment. We thank NSERC (Natural Sciences and Engineering Research Council of Canada) for financial support, and Drs. R. McDonald and M. J. Ferguson, University of Alberta, for X-ray structural data.

Supporting Information Available: X-ray crystallographic data in CIF format for **1**−**5**. This material is available free of charge via the Internet at http://pubs.acs.org.

IC0206950

(33) Kwak, N.; Rhee, H.; Park, S.; Lah, M. S. *Inorg. Chem.* **1998**, *37*, 3599.
(34) Moon, M.; Kim, I.; Lah, M. S. *Inorg. Chem.* **2000**, *39*, 2710.
(35) Eshel, M.; Bino, A.; Felner, I.; Johnston, D. C.; Luban, M.; Miller, L. L. *Inorg. Chem.* **2000**, *39*, 1376.
(36) McInnes, E. J. L.; Anson, C.; Powell, A. K.; Thomson, A. J.; Poussereau, S.; Sessoli, R. *J. Chem. Soc., Chem. Commun.* **2001**, 89.
(37) Dearden, A. L.; Parsons, S.; Winpenny, R. E. P. *Angew. Chem., Int. Ed.* **2001**, *40*, 152.